

Patch-Grid: An Efficient and Feature-Preserving Neural Implicit Surface Representation

GUYING LIN*, The University of Hong Kong, China
 LEI YANG*[†], The University of Hong Kong, China
 CONGYI ZHANG, The University of Hong Kong, China
 HAO PAN, Microsoft Research Asia, China
 YUHAN PING, The University of Hong Kong, China
 GUODONG WEI, The University of Hong Kong, China
 TAKU KOMURA, The University of Hong Kong, China
 JOHN KEYSER, Texas A&M University, United States of America
 WENPING WANG[†], Texas A&M University, United States of America

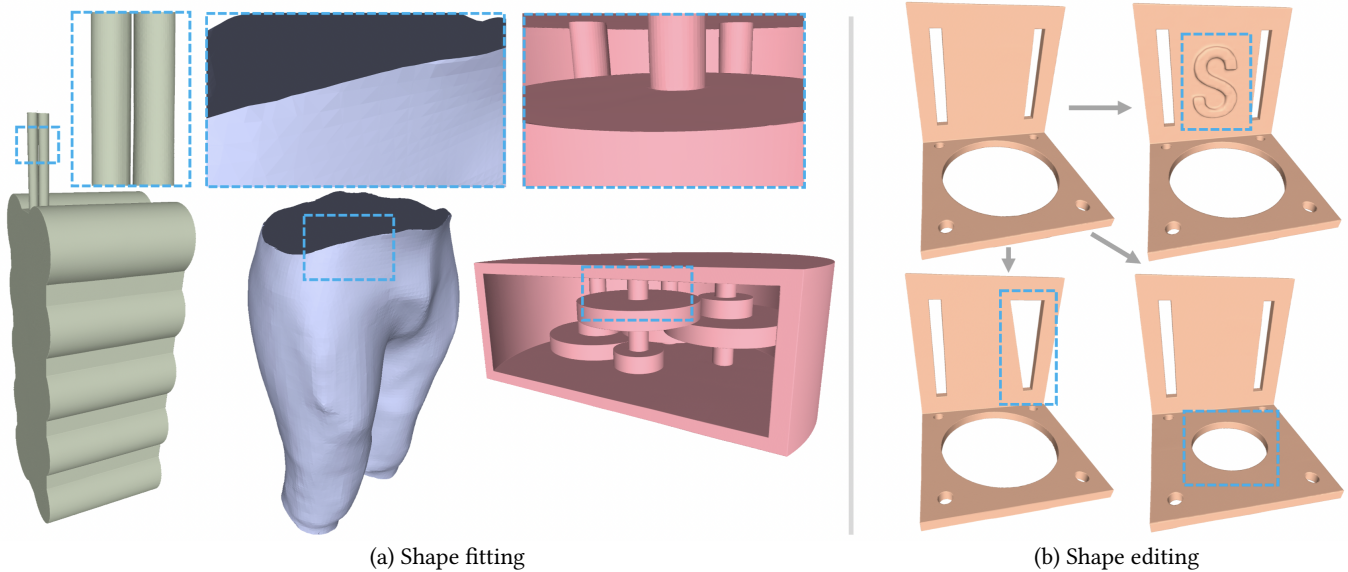


Fig. 1. Our *Patch-Grid* method is capable of (a) modeling diverse geometric features, such as thin geometric features, open surface boundaries, and sharp features (from left to right); (b) *Patch-Grid* also allows updating a thus learned implicit representation to incorporate bump textures (top right) or reshape a geometric feature (bottom) within 1 second.

Neural implicit representations are increasingly used to depict 3D shapes owing to their inherent smoothness and compactness, contrasting with traditional discrete representations. Yet, the multilayer perceptron (MLP) based neural representation, because of its smooth nature, rounds sharp corners or edges, rendering it unsuitable for representing objects with sharp features like CAD models. Moreover, neural implicit representations need

long training time and struggle to represent surfaces with open boundaries. While previous works address these issues separately, we present a unified neural implicit representation called *Patch-Grid*, which fits to complex shapes efficiently, preserves sharp features delineating different patches and can also represent surfaces with open boundaries and thin geometric features. The efficiency of *Patch-Grid* comes from encoding each patch with a local grid of spatial latent codes and adaptive resolution, called the *patch feature volume*, coupled with an MLP decoder mapping grid features to implicit function values. The MLP decoder is shared among all the patch feature volumes and pretrained on a broad variety of local surface geometries; given the pretrained and fixed MLP decoder, novel shapes and local updates can be fitted efficiently by optimizing the patch feature volumes with high flexibility and locality. The faithful preservation by *Patch-Grid* of sharp edges and corners is enabled by constructive solid geometry (CSG) combinations of patches. To merge the patches with robust CSG operations to produce sharp features, we propose a *merge grid* that embeds the different patch

*Both authors contributed equally to this research.

[†]Corresponding authors.

Authors' addresses: Guying Lin, guyinglin2000@gmail.com, The University of Hong Kong, Hong Kong, China; Lei Yang, l.yang@transp.hk, The University of Hong Kong, Hong Kong, China; Congyi Zhang, zhcy@outlook.com, The University of Hong Kong, Hong Kong, China; Hao Pan, haopan@microsoft.com, Microsoft Research Asia, Beijing, China; Yuhan Ping, csyhping@connect.hku.hk, The University of Hong Kong, Hong Kong, China; Guodong Wei, g.d.wei.china@gmail.com, The University of Hong Kong, Hong Kong, China; Taku Komura, taku@cs.hku.hk, The University of Hong Kong, Hong Kong, China; John Keyser, keyser@cse.tamu.edu, Texas A&M University, College station, United States of America; Wenping Wang, wenping@tamu.edu, Texas A&M University, College station, United States of America.

grids in a common octree structure, and forms CSG combinations locally to achieve better robustness than using a global CSG construction.

Experiments show that our *Patch-Grid* representation accurately captures shapes with complex sharp features, open boundaries and thin geometric features, and outperforms existing learning-based methods in efficiency for surface fitting and local shape updates.

1 INTRODUCTION

The implicit surface representation typically defines a shape as the zero-level set of some function, such as the signed distance function of the shape. The implicit representation is widely used for shape modeling [Mitchell et al. 2015; Ohtake et al. 2005; Turk and O’Brien 2002] and downstream engineering applications like simulation [Allen 2021]. Recent years have seen a surge in research on *neural implicit representations* [Gropp et al. 2020; Martel et al. 2021; Park et al. 2019; Tancik et al. 2020b] where a deep neural network is used to encode the implicit function in question. Neural implicit representations are inherently smooth and can represent complex shape details more compactly than traditional discrete representations, e.g. point clouds and polygonal meshes [Sitzmann et al. 2020b; Takikawa et al. 2021].

There are two main challenges with current neural implicit surface representations. First, they struggle to represent a variety of geometric features, such as sharp geometric edges, surfaces with open boundaries, and surfaces whose parts form narrow gaps; see some examples in Fig. 1. While there have been some recent attempts to address individual challenges, such as merging a set of neural half-spaces to model sharp geometric edges [Guo et al. 2022] or additionally predicting a mask for extracting open surface boundaries [Chen et al. 2022], there is no *unified framework* capable of faithfully representing these geometric features in shape modeling.

Second, learning a neural implicit representation to accurately fit a given shape often takes excessively long time, from minutes to around an hour, precluding its application to interactive design. While modern hardware and algorithmic improvement have been proposed to substantially reduce the training time of neural implicit representations [Müller et al. 2022], there is still a demand for faster methods to efficiently model neural implicit surfaces and update existing ones by interactive editing.

To tackle these two challenges, we present *Patch-Grid*, a compositional framework for modeling neural implicit surfaces with two distinctive advantages: 1) **Versatile representation**: it can represent sharp geometric features, open surface boundaries, and thin geometric features (such as slender tubes or narrow gaps), which are challenging or impossible for current neural surface representations, as shown in Fig. 1; 2) **Superior efficiency**: *Patch-Grid* is faster to train than current neural representations. It typically takes about 8 seconds to train *Patch-Grid* to fit a given shape and about 1 second to complete a local shape update of an existing surface represented by *Patch-Grid*. This enables interactive editing of neural implicit surfaces.

The problem we address is formulated as follows. Given a boundary representation (B-Rep) of a 3D shape, which defines the 3D surface shape as a set of surface patches, we aim to convert this B-rep representation into a neural implicit representation, by representing each surface patch as a zero-level set of a neural implicit

function. Specifically, each surface patch is tightly contained in a truncated volume that comprises a regular grid of cubic cells with a learnable feature vector assigned to each grid point.

The collection of these grid cells is referred to as the *patch volume* and the collection of feature vectors defined on it is referred to as the *patch feature volume* of the surface patch. For any point x inside a cubic cell, a 3-layered MLP (Multi-Layer Perceptron) decoder is used to map the feature vector at x , which is obtained via trilinear interpolation from feature vectors at the corners of the cell, to a signed distance value, as shown in Fig. 2.

We observe that the global CSG approach adopted by *NH-Rep* [Guo et al. 2022] for the same task often leads to failure cases in highly concave and narrow regions because multiple surface patches need to be carefully merged in a global manner to avoid undesired interference (cf. Fig. 4). Since the intersection of two or more surface patches forming a sharp geometric feature (edges or corners) is only a local operation, we propose to use a *merge grid* for robustly modeling sharp features of a given shape in a local manner. Specifically, the merge grid uses an octree structure to adaptively subdivide the spatial domain into cubic cells so that each leaf cell ideally contains no more than *one* sharp feature to simplify the task. Therefore, our approach circumvents the difficulty in merging multiple patches into various sharp features globally [Guo et al. 2022] by adopting a divide-and-conquer strategy for merging multiple patches in a local region, thereby achieving robust and superior performance for modeling various geometric features as shown in Fig. 1.

Besides sharp features, our local approach is also capable of modeling **thin geometric features** and **open surface boundaries**. In a general sense, a slender tube or a narrow gap/slit is considered a thin geometric feature (e.g. columns 1,2,4 in Fig. 15). By adopting a local approach, *Patch-Grid* robustly models *thin geometric features* by placing spatially proximal but disjoint surface patches in different patch volumes which may overlap. In this way, the distance fields induced by the different surface patches do not interfere with each other, thereby enabling the modeling of narrow gaps or thin solids formed by these surface patches. Furthermore, we model a boundary curve of an open surface patch as a result of the trimming operation. Therefore, modeling a boundary curve amounts to constructing a trimming surface followed by a trimming operation, which can be performed locally to produce accurate results.

Efficiency. Even without using a sophisticated CUDA implementation, the proposed approach that uses patch-level feature vectors and a merge grid for modeling geometric features can achieve high training efficiency. Typically, our method takes about 8 secs to fit a given shape from scratch and supports local shape updates at an interactive rate (about ~ 1 sec). We will release our code.

In summary, the contributions of this paper are:

- *Versatile representation.* We present *Patch-Grid*, a compositional neural implicit representation capable of modeling a variety of geometric features, such as sharp or thin geometric features and open boundaries, that are challenging for previous methods;
- *Robustness.* A novel *merge grid* is proposed that adaptively partitions the spatial domain and locally composes neural implicit surface patches to faithfully model a target surface

shape with sharp features (i.e. edges and corners) in a more robust manner than the existing global approach [2022].

- *Superior efficiency.* We present an efficient implementation of *Patch-Grid* which consists of 1) an adaptive patch feature volume and 2) a merge octree to simplify the merge constraints. Combined with a pretraining strategy, this allows *Patch-Grid* to achieve a very fast training time (in several seconds) and support local shape updates at an interactive rate (~ 1 sec), which is much faster than all the existing methods for modeling neural implicit surfaces.

2 RELATED WORKS

2.1 Global implicit representation

Neural implicit representation is a novel approach that turns traditional explicit discrete representations (e.g. point clouds, polygon meshes, or voxels) into the iso-surface of some continuously defined differentiable fields represented through a neural network [Chen and Zhang 2019; Mescheder et al. 2019; Park et al. 2019]. To improve the performance when overfitting the network to complex 3D shapes, a series of techniques have been proposed, such as exploring the optimal hyper-parameters [Davies et al. 2020], training strategies [Duan et al. 2020], positional encoding [Tancik et al. 2020a], and sinusoidal activation [Sitzmann et al. 2020b]. Another line of work focuses on extending the capability of neural implicit representations to general shapes like open surfaces, such as neural unsigned distance field [Chibane et al. 2020], or modified SDF [Chen et al. 2022]. However, these prior approaches cannot faithfully recover sharp features or cannot scale between fine-grained shapes and large scenes.

2.2 Grid- or Patch-based implicit representation

A direct improvement on standard, global, implicit representation is to build spatial grids [Jiang et al. 2020] or octrees [?] to split the original shape fitting problem into a set of subproblems. However, due to the grid-based representation strategy, the surface between grids may not be smoothly connected.

Representing the entire shape using a set of shape primitives is a classic point of view in traditional explicit geometry processing [Li et al. 2011; Nan and Wonka 2017; Schnabel et al. 2007]. Those patch-wise representations decompose complex models into multiple patches with parametric shape priors to extract high-level shape structures for downstream applications like shape completion or semantic editing. Motivated by the simplicity of patches, neural implicit representations adopted similar ideas to decompose shapes, allowing learning of locally controllable models [Genova et al. 2020], generalizable parts [Tretschk et al. 2020], or a semantic compositional parametric model [Zhang et al. 2022]. However, it is not easy to achieve high representation accuracy by using patch-based implicit representations, due to the difficulty in stitching together or trimming patches.

Focusing on neural implicit modeling of CAD shapes with sharp features, Guo et al. [2022] give a global CSG-based solid entity representation that is based on patch-wise halfspaces. They first propose a top-down constructive method to build the global CSG tree that ensures the order of Boolean operations yields theoretically sound

results. Then they supervise learning patch-wise halfspace-based representations on all sample points in the domain, thus coordinating them in the whole space. As we will show in experiments, in contrast to our local approach to CSG construction for sharp feature modeling, the global approach has difficulty precisely representing complex shapes with many concave patches. Moreover, our approach handles more general surface types than solid CAD shapes, including open surfaces, self-intersecting surfaces, and non-orientable surfaces.

3 OUR METHOD

3.1 Overview

We present the overview pipeline of *Patch-Grid* in Fig. 2. Input to our method is a shape $\mathcal{S} = \bigcup_{p=1}^K S_p$ composed of a collection of surface patches S_p along with the type of connection between adjacent patches. Our goal is to represent the shape \mathcal{S} as a neural implicit surface \mathcal{Z} composed of a collection of neural signed distance fields. We denote the zero-level set of a neural signed distance field as Z_p which contains a target surface patch S_p . To facilitate fast training and effective modeling, we introduce a patch volume for each surface patch S_p to tightly bound S_p and define the extent of Z_p as shown in Fig. 2(b). Furthermore, we impose a regular grid structure on the patch volume of S_p and assign a feature vector at each grid point. Then the collection of all these feature vectors is referred to as the *patch feature volume*. Here, the grid resolution is determined by the local shape complexity, as to be explained later. The use of the patch feature volume allows us to use an MLP to map an interpolated feature vector at a query coordinate to a signed distance value, approximating the SDF of the surface patch S_p (Sec. 3.2).

We use a local approach based on another grid structure, named merge grid \mathcal{G} , to effectively assemble $\{Z_p\}_{p=1}^K$ into the final neural representation \mathcal{Z} . The merge grid adaptively subdivides the spatial domain around the sharp geometric features, so as to simplify the adjacency graph of surface patches enclosed in the individual merge grid cells (Sec. 3.3). A patch volume and the merge grid of a 3D shape are shown in Fig. 3. With this localized representation, the overall training process is presented in Sec. 3.4. We further present a strategy to achieve local shape update in Sec. 3.5.

3.2 Patch Feature Volumes

We will introduce *patch feature volumes* to represent individual surface patches. For each surface patch S_p of a given shape, we first determine its axis-aligned rectangular bounding box and partition the bounding box into a grid of regular rectangular cells, whose size is determined adaptively according to the shape complexity of the patch. Then, we prune the cells to keep only those that enclose part of the surface patch S_p , so that the union of these remaining nonempty cells forms a tight bounding volume of S_p , which is called a *patch volume* and denoted by V_p , as shown in Fig. 3(b).

Next, for each patch volume, we introduce a learnable *feature volume*, $FV_p = \{f_{(i,j,k)}^p\}$, where each $f_{(i,j,k)}^p \in \mathbb{R}^D$ is assigned to a grid point indexed by (i, j, k) . Then a feature field $F_p(\mathbf{x}) : V_p \rightarrow \mathbb{R}^D$ is defined in the patch volume V_p by trilinear interpolation of the

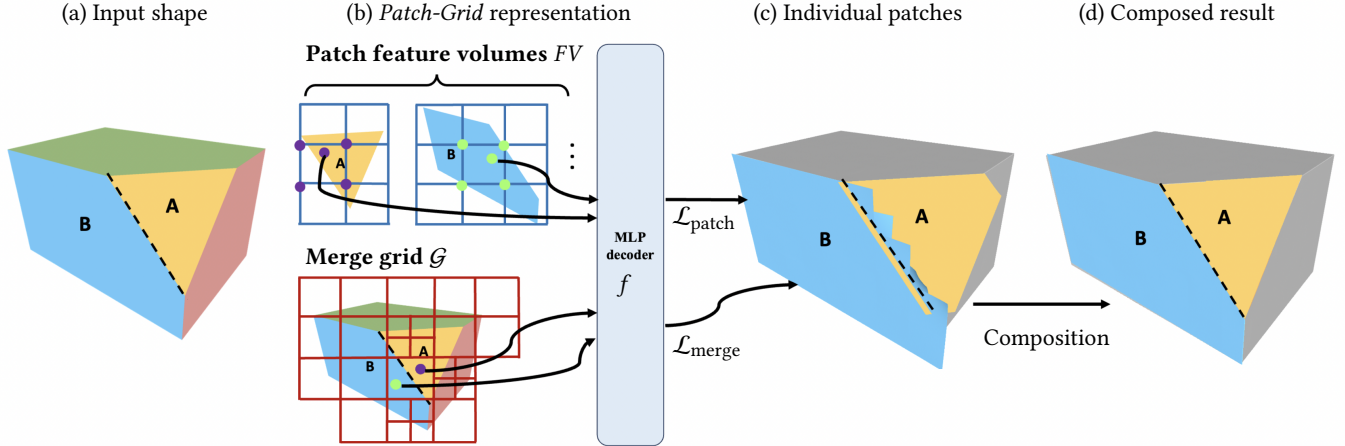


Fig. 2. Overview of the proposed *Patch-Grid* representation. (a) Input to our method is a B-rep model of a 3D shape \mathcal{S} ; (b) *Patch-Grid* bounds each surface patch of the given shape with a patch volume. We assign a learnable feature vector \mathbf{v}_i to each corner point of the patch volume and convert this volume into a patch feature volume FV , which defines a continuous feature field $F(\mathbf{x})$ via trilinear interpolation within each cubic cell. Then, a shared MLP decoder f is used to map $F(\mathbf{x})$ to represent the SDF of the target surface patch. To merge the individual patches together, we construct a merge grid \mathcal{G} and enforce a merge loss within each of the merge grid cells; (c) We design two types of loss terms to enable accurate fitting of individual patches ($\mathcal{L}_{\text{patch}}$) and model the relationship between connected patches ($\mathcal{L}_{\text{merge}}$), respectively; (d) Finally, the individual neural surface patches are composed into the final surface shape that reconstructs the target shape. It takes 8 secs to fit this example.

feature vectors at the 8 corner points of the cell containing the spatial query point $\mathbf{x} \in \mathbb{R}^3$. The grid resolution is determined adaptively according to the shape complexity of individual patches. Specifically, it is based on the averaged shape diameter function [Shapira et al. 2008], which is a reasonable approximation of the local feature size [Amenta and Bern 1998].

Given the continuous feature vector field $F_p(\mathbf{x})$, we use an MLP decoder f to represent surface patch S_p as part of the zero-level set Z_p of the following function,

$$S_p \subset Z_p = \{\mathbf{x} | f(F_p(\mathbf{x})) = 0\}. \quad (1)$$

The surface shape thus generated is independent of the absolute position of the query point but depends solely on the interpolated features $\mathbf{v}(\mathbf{x})$. The use of the patch feature volume allows the decoder f to be pretrained on a shape dataset to learn a local shape prior, as we will explain in Sec. 3.5.

Representing a surface patch in a local domain defined by the patch volume is a key design that distinguishes our method from the global approach used in [Guo et al. 2022]. In this way, each learned implicit function of a surface patch is only defined within the patch volume as shown in Fig. 2(c). This effectively trims off the extraneous zero-level set of a learned implicit function outside the patch volume and hence avoids the difficulty of managing extraneous zero-level sets faced by the global approach.

For the remaining extraneous zero-level sets within the patch volumes V_p , we need to merge Z_p with its neighboring patches following a sequence of pre-defined Boolean operations, i.e., a CSG tree, to form S_p , as will be represented next.

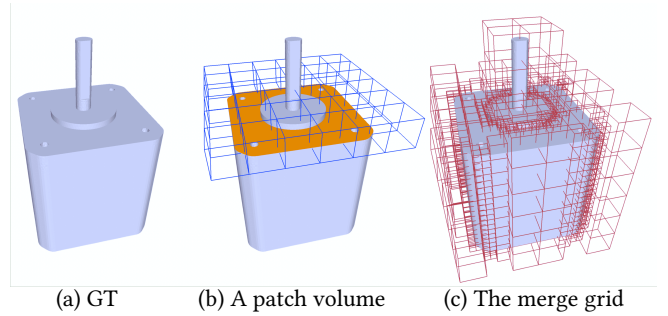


Fig. 3. Given a 3D shape (a), a patch volume of the patch in orange in (b) and the merge grid in (c) are shown.

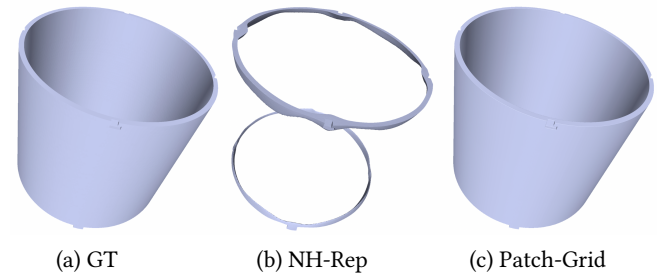


Fig. 4. (a) A challenging case with some highly concave regions at the top and bottom of the cylindrical shell. (b) *NH-Rep* fails in this challenging case due to the difficulty in merging the learned implicit functions in a global manner. (c) Our *Patch-Grid* performs robustly due to the localized approach adopted.

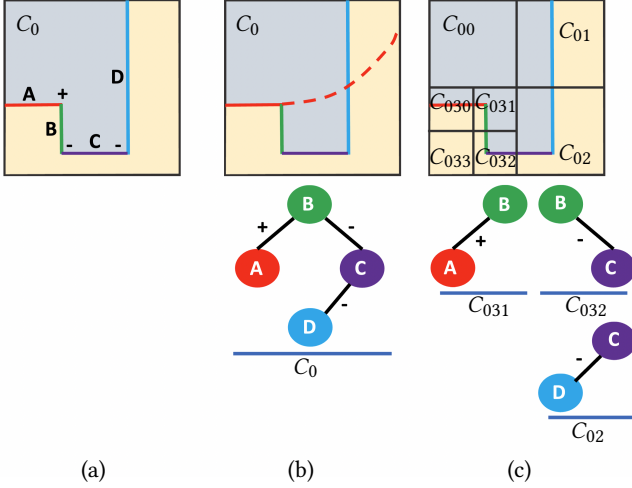


Fig. 5. (a) Target geometry (mellow yellow) bounded by four patches A , B , C and D . The CSG tree is provided for this example. Convex sharp connections between the patches are denoted $+$ while concave connections are denoted with $-$; (b) A failure case due to the undesired interference of the extraneous zero-level set of the patch A to the patch D ; (c) Subdividing cell C_0 into cells C_{0i} ($i = \{0, 1, 2, 3\}$) and then subdividing cell C_{03} into cells C_{03j} ($j = \{0, 1, 2, 3\}$). Each subdivided cell now contains at most one sharp feature in it.

3.3 Merge Grid and Merging Constraints

To form a sharp boundary edge shared by two adjacent patches, a Boolean operation (max for intersection or min for union) is utilized depending on whether the sharp edge is convex or concave. The adjacency of two connected patches forming a sharp convex edge is denoted as $+$, indicating the max operation; otherwise, the adjacency is concave, denoted by $-$, indicating the min operation. Hence, a CSG tree can be used to define a sequence of Boolean operations that assemble multiple surface patches into the target shape. In contrast to the global approach to constructing this CSG tree [Guo et al. 2022], which is prone to suffer from the robustness issue (see Fig. 4 for an example), we adopt a local approach based on an adaptive *merge grid* \mathcal{G} to improve the robustness of our learned neural implicit representation.

Global approach lacks robustness. We will use a simple 2D example in Fig. 5 to illustrate the robustness issue encountered by the global approach. Consider a 2D solid shape (shaded in mellow yellow) bounded by four curve segments A , B , C and D , with two sharp geometric features, i.e., corners in 2D. Its global CSG tree is shown on the right. Because of the loss of control over the extraneous zero-level set of the curve segment A (the red dashed curve), undesired interference between the curve segments A and D in the global domain result in an artifact in the reconstructed shape as shown in Fig. 5(b). This simple 2D example helps explain the robustness issue in the 3D case facing the global approach presented in *NH-Rep* [Guo et al. 2022], which often fails in highly concave regions that involve multiple patches, because of the essentially same reason due to the loss of control on unintended interference

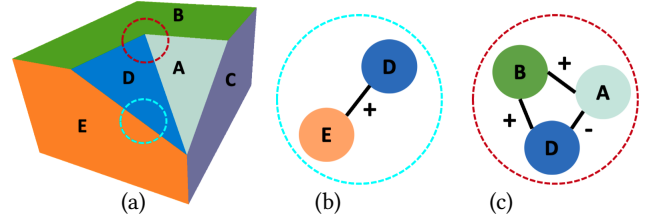


Fig. 6. Sharp geometric features in a 3D shape. (a) A 3D example; (b) The adjacency graph of an edge feature; (c) The adjacency graph of a corner feature.

between the extraneous zero-level sets of some unconnected surface patches, as shown in Fig. 4 for example.

Adaptive merge grid. To overcome this robustness issue, we adopt a divide-and-conquer strategy by subdividing the spatial domain with an adaptive merge grid. Let us continue our explanation with the aforementioned 2D example. By subdividing the spatial domain (denoted C_0) in Fig. 5(a), each subdivided cell in Fig. 5(c) contains a simpler geometry – at most one sharp corner is enclosed in each cell. The benefit is two-fold. First, the curve segment D is now defined only in cell C_{01} and C_{02} and so is its extraneous zero-level set. This circumvents the demanding task of managing extraneous zero-level sets of multiple patches in a global manner. Second, the construction of the sharp corner formed by C and D (in C_{02}) now involves only these two relevant patches, while the curve segment A is trimmed off in C_{031} avoiding any potential interference from other unconnected patches (e.g., A) as opposite to what is shown in Fig. 5(b). This localized approach drastically improves the robustness of CSG operations as compared with the global approach.

Now, we elaborate on this subdividing scheme for 3D shapes. Consider each patch as a node. An undirected *adjacency graph* can be defined for the patches bounded in each domain. Then, a sharp edge formed by two adjacent patches corresponds to a link in the adjacency graph and a corner feature at which multiple patches intersect corresponds to a complete subgraph of the adjacent graph, as shown in Fig. 6. We initialize the merge grid as an octree grid with the initial resolution the same as the finest resolution of the patch volume. Then, each non-empty leaf cell of the merge grid is recursively subdivided unless the adjacency graph of the cell is a complete graph. This is because any subdivision of this cell will not further simplify the CSG operations required to form such a geometric feature. The pseudo-code for constructing such an adaptive merge grid is provided in Alg. 1.

Once the merge grid has been adaptively subdivided, we first construct a CSG tree based on the adjacency graph of each non-empty leaf cell of the merge grid. Then, we follow Boolean operations in the CSG tree to constrain the learned implicit functions such that the zero-level set of the merged implicit function M reproduces the target geometry. Specifically, we define the merge loss $\mathcal{L}_{\text{merge}}^i$ in non-empty leaf cell C_i as follows

$$\mathcal{L}_{\text{merge}}^i = \sum_{\mathbf{x} \in \cup_p \{S_p\} \cap C_i} |M(\mathbf{x})|. \quad (2)$$

where \mathbf{x} are sampled from the surface patches within the cell C_i .

Algorithm 1 Construction of Merge Grid

Input:
 Surface shape \mathcal{S}
 Initial merge grid \mathcal{G}
 Maximal depth d_{max} ;

Output:
 Merge grid \mathcal{G} ;

```

1: while #subdivisible leaf cells > 0 do
2:   for  $C \in \mathcal{G}$  do
3:     if  $C.sub == False$  then
4:       continue;
5:     else if  $\mathcal{S} \cap C \neq \emptyset$  or  $C.d < d_{max}$  then
6:       for every connected graph  $g$  in  $C$  do
7:         if  $g$  is not a clique graph then
8:            $S \leftarrow subdivide(C)$ ;
9:            $C.sub \leftarrow True, \forall C \in S$ ;
10:          break;
11:         end if
12:       end for
13:        $C.sub \leftarrow False$ ;
14:       {/*clique cell*/}
15:     else
16:        $C.sub \leftarrow False$ 
17:       {/*empty cell or cell reaches  $d_{max}$ */}
18:     end if
19:   end for
20: end while

```

3.4 Learning Patch-Grid Representation

The patch feature volumes $\{FV_p\}_{p=1}^K$ and the weights of the shared decoder f are trainable parameters and optimized to fit the target shape \mathcal{S} . We adopt a surface fitting loss $\mathcal{L}_{surface}$ and a surface normal fitting loss \mathcal{L}_{normal} as the data terms for the fitting loss. Besides, we also adopt a pseudo SDF loss \mathcal{L}_{SDF} and a pseudo gradient loss $\mathcal{L}_{gradient}$ to improve the quality of the fitting results. Two regularization terms are employed, namely the Eikonal term $\mathcal{L}_{eikonal}$ proposed in [Gropp et al. 2020] and an off-surface penalty term \mathcal{L}_{off} used in [Sitzmann et al. 2020a]. We further impose an l_2 regularization \mathcal{L}_{code} on the feature volumes. Hence, the loss function for learning each patch is defined as

$$\begin{aligned} \mathcal{L}_{patch} = & \lambda_{surface} \mathcal{L}_{surface} + \lambda_{normal} \mathcal{L}_{normal} \\ & + \lambda_{SDF} \mathcal{L}_{SDF} + \lambda_{gradient} \mathcal{L}_{gradient} \\ & + \lambda_{off} \mathcal{L}_{off} + \lambda_{Eikonal} \mathcal{L}_{Eikonal} + \lambda_{code} \mathcal{L}_{code}, \end{aligned} \quad (3)$$

where

$$\mathcal{L}_{surface} = \sum_{\mathbf{x} \in S_p} |f(F_p(\mathbf{x}))|, \quad (4)$$

$$\mathcal{L}_{normal} = \sum_{\mathbf{x} \in S_p} \|\nabla_{\mathbf{x}} f(F_p(\mathbf{x})) - \mathbf{n}(\mathbf{x})\|_2, \quad (5)$$

$$\mathcal{L}_{SDF} = \sum_{\mathbf{x} \in S_p} |f(F_p(\mathbf{x} + d\mathbf{n})) - d|, \quad (6)$$

$$\mathcal{L}_{gradient} = \sum_{\mathbf{x} \in S_p} \|\nabla_{\mathbf{x} + d\mathbf{n}} f(F_p(\mathbf{x} + d\mathbf{n})) - \mathbf{n}(\mathbf{x})\|_2, \quad (7)$$

$$\mathcal{L}_{off} = \frac{1}{|\Omega_p|} \sum_{\mathbf{x} \in \Omega_p} \exp(|-0.01f(F_p(\mathbf{x}))|), \quad (8)$$

$$\mathcal{L}_{Eikonal} = \frac{1}{|\Omega_p|} \sum_{\mathbf{x} \in \Omega_p} \left| \|\nabla_{\mathbf{x}} f(F_p(\mathbf{x}))\| - 1 \right|, \quad (9)$$

$$\mathcal{L}_{code} = \frac{1}{K \cdot |V_p|} \sum_{i=1}^K \sum_{j,k} \|v_{i,j,k}^p\|_2^2. \quad (10)$$

Here, $\mathbf{n}(\mathbf{x})$ denotes the unit normal vector at \mathbf{x} ; d is a small offset distance with a range $(0, 0.1)$ of the grid cell size; and Ω_p denotes the set of point samples from the patch volume of surface patch S_p .

The final loss of the optimization problem takes the following form:

$$\mathcal{L}_{total} = \frac{1}{K} \sum_{p=1}^K \mathcal{L}_{patch}^k + \lambda_{merge} \frac{1}{L} \sum_{i=1}^L \mathcal{L}_{merge}^i. \quad (11)$$

where L denotes the number of the non-empty leaf cells in \mathcal{G} .

3.5 Fast Local Shape Updating with Pretrained Decoder

Editing is an important means of 3D shape modeling. In CAD modeling, users could adjust the size of a component or deform its geometry to edit an existing 3D model. Therefore, it would be desirable if the learned representation can be updated as the CAD model is edited at an interactive rate, as opposed to the existing methods [Guo et al. 2022; Martel et al. 2021; Takikawa et al. 2021] that can only overfit the edited shape from scratch, which takes too long time for interactive editing.

To speed up the retraining process, we leverage the compositional nature of *Patch-Grid* and develop a new strategy to enable a fast local update within 1 second. The overall idea is to perform a test-time optimization that only optimizes the patch feature volumes of the edited patches while fixing all other patch feature volumes as well as the shared MLP decoder f . This local updating strategy thus reduces the computational time significantly to allow interactive local shape update.

In order to realize the above idea, the shared MLP decoder f needs to be sufficiently pretrained. To acquire a local shape prior, we pretrained the decoder f on a set of 500 patches randomly cropped from 25 shapes that exhibit diverse geometric details. During the pretraining stage, given a patch S_p from a shape, we construct its patch volume V_p and randomly initialize the patch feature volume FV_p as described earlier. The decoder f along with the patch feature volume FV_p are trained to reconstruct the corresponding surface patch S_p during the pretraining process using Eq. 3. This process

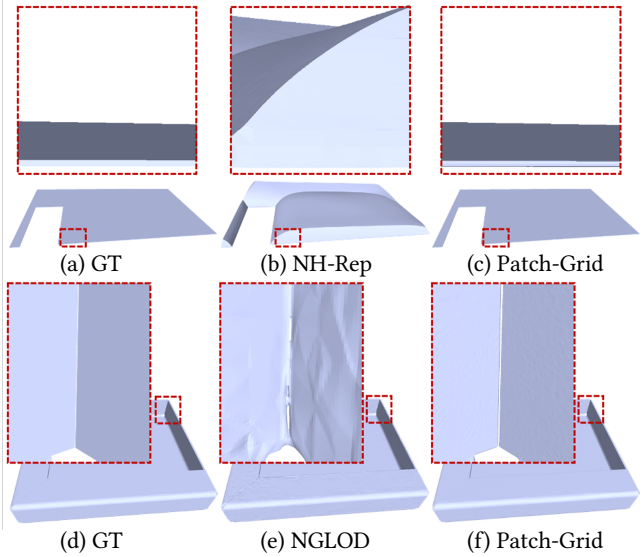


Fig. 7. Modeling of thin structures. Due to their global scheme, *NGLOD* and *NH-Rep* struggle to represent thin structures; however, our localized method robustly and faithfully addresses these challenging cases.

exposes the decoder f to a diverse collection of surface patches and thus instills a local shape prior into the decoder f . As will be shown in the experiment, the well-learned local shape prior can serve as a strong shape bias for the test-time optimization of the feature codes in FV_p and a high-quality local update result can be obtained with 100 iterations or 1 second.

While we only pretrain the decoder f on a fixed-resolution grid (8^3 in our implementation), the pretrained decoder can generalize well to grids with higher resolutions. This is partly because grid cells at a higher resolution usually contain simpler geometry (with a low curvature). Hence, when the edited patch becomes more complicated (as indicated by its averaged shape diameter function), we can increase the resolution of the patch volume V_p and still use the same decoder for test-time optimization.

4 MODELING DIVERSE GEOMETRIC FEATURES

In this section, we introduce how the proposed *Patch-Grid* representation can be applied to modeling diverse geometric features, such as narrow slits or thin solids (which are together termed as thin geometric features here), open surface boundaries, and enabling global distance query via a local-global blending scheme.

4.1 Modeling of Thin Geometric Features

It is challenging for a global approach like *NH-Rep* [Guo et al. 2022] or *NGLOD* [Takikawa et al. 2021] to fit a neural implicit representation to a 3D shape with thin geometric features, such as the thin solid shown in Fig. 7 (upper row) and the very thin gap shown in Fig. 7 (bottom row). On the one hand, insufficient samples around these thin features, coupled with the inherent difficulty that the MLP faces in handling sharp changes in SDF, accounts for the failures encountered in such regions by *NGLOD* [Takikawa et al. 2021].

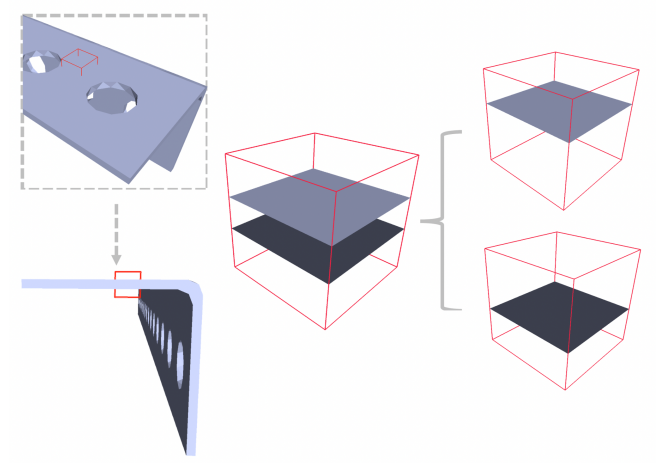


Fig. 8. Processing thin geometric features. Each of the two surface patches bounding the thin solid is modeled by a separate independent neural signed distance field.

On the other hand, *NH-Rep* [Guo et al. 2022], while being a patch-based representation, is limited by the global approach it adopts. As described earlier, the need for managing global interaction between all pairs of patches makes it prone to fail to model the thin features, as shown in the top of Fig. 7.

In contrast to previous methods, our *Patch-Grid* locally represents each composing surface patch with a bounding patch volume and achieves robust results in regions of thin geometric features; see our results in Fig. 7. We demonstrate how our local representation benefits the modeling of thin geometric features with Fig. 8 where a thin solid is bounded by two spatially close yet disconnected surface patches. First, the two surface patches are separately represented by their respective patch volumes, and so are their signed distance fields. Therefore, learning the two *individual* signed distance fields avoids excessively dense sampling around the thin solid as required by *NGLOD*. On the other hand, while it adopts a similar patch-based representation, *NH-Rep* defines the patches in the global domain and can only evaluate the geometry through the CSG tree in a global manner that struggles to disentangle the two disconnected but almost overlapping patches. In contrast, our *Patch-Grid* enables local evaluation of a surface patch within its patch volume. If two patches are not connected (see Fig. 8), each surface patch can be individually extracted without going through the CSG tree. Hence, our local approach exhibits high flexibility in modeling these thin geometric features.

4.2 Modeling of Open Surface Boundaries

The modeling of an open surface boundary can be considered as a trimming process, where the open surface patch is formed by trimming an extended surface at the boundary curve with a trimming surface. An example is illustrated in Fig. 9. We denote a given open surface as S_o and its boundaries as ∂S_o .

We follow the method presented earlier to train a neural surface patch Z_o that reconstructs S_o with some extraneous part (see Eq. (1)). To represent the trimming surface as a zero-level set of a neural

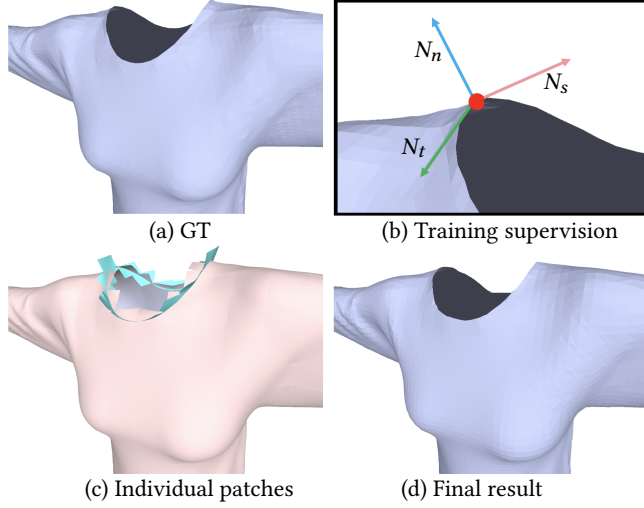


Fig. 9. Modeling open boundary surfaces. To learn the trimming patch, the normal supervision N_s is obtained by computing the cross product of the surface normal N_n and the tangent vector of the boundary N_t .

implicit function, we need to provide sample points in the zero-level set and gradient directions at these points.

Specifically, we first sample from the boundary curve ∂S_o a set of points \mathbf{x}_b at which the zero-level set of the trimming surface passes through. Then, we compute at each of these sampled points a vector N_s that represents the gradient direction of the target implicit functions. N_s is computed as the cross product of the surface normal N_n at this point and the tangent N_t along the boundary curve ∂S_o as shown in Fig. 9(b). Pseudo SDF and gradients are hence computed from \mathbf{x}_b and $N_s(\mathbf{x}_b)$. We adopt the same training loss, Eq. (3), to obtain a learned implicit function serving as the trimming patch. The zero-level set of the trimming patch is then used to cut off the extraneous part of the zero-level set Z_o to form a clean boundary curve.

We implement this trimming operation as a Boolean max operation, assuming that the trimming surface and the corresponding open surface form a sharp convex feature at the boundary curve. Hence, we can adopt the same pipeline as described before to model this virtual sharp edge. During mesh extraction, we simply mask out the sample triangles lying on the trimming surface. We show several results of the modeled open surfaces along with zoom-in views at the surface boundaries in Fig. 18.

4.3 Enabling global distance query

CAD applications often require a global signed distance function to support inquiring whether a given point is inside or outside of a CAD model. To address this issue, we extend our local patch-based surface representation to a *feature-preserving* global signed distance field F_G for CAD models by blending the local patch-based representation F_L with an ordinary global signed distance field F_O . A 2D example is shown in Fig. 10 where the GT shape contains a sharp corner. The patch-based representation F_L is defined only in a region nearby the GT surface, while the learned global field F_O smoothly approximates the sharp corner in the GT shape. A blended

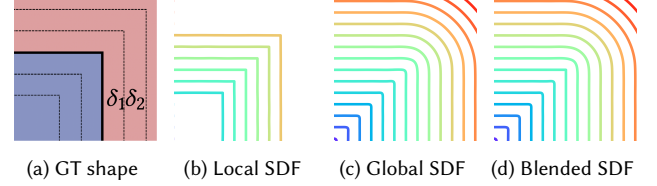


Fig. 10. Given the blending region around the GT shape (a), the local SDF (b) and the global SDF (c) are blended to generate the blended SDF (d) that well preserves the sharp corner at its zero-level set and is globally defined in the whole domain.

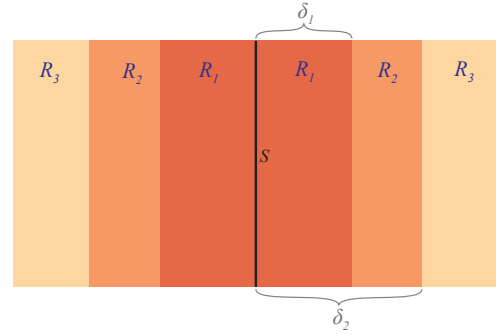


Fig. 11. We demonstrate the blending strategy in a 2D case.

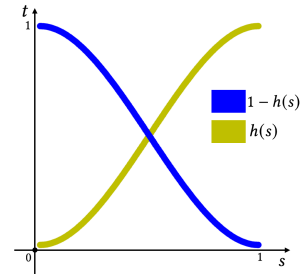


Fig. 12. Weight functions for smooth interpolation.

field obtained by the following method can retain the sharp feature in the GT shape as well as enable a global distance query.

With F_L being a sufficiently accurate distance value for points near the surface S , we define three regions as follows: the region $R_1 = \{\mathbf{x} \mid |F_L(\mathbf{x})| < \delta_1\}$, $R_2 = \{\mathbf{x} \mid \delta_1 \leq |F_L(\mathbf{x})| \leq \delta_2\}$, and $R_3 = D \setminus (R_1 \cup R_2)$, where D is the entire bounding domain $([-1, 1]^3)$ of a given shape. Then, we design the global feature-preserving distance function F_G . Inside the region R_1 , we set $F_G = F_L$, because the local distance function F_L is accurate and feature-preserving in R_1 . In our implementation, with all shape bounding boxes as $[-1, 1]^3$, we choose $\delta_1 = 0.001$ in the definition of R_1 . In R_3 , since F_L becomes inaccurate and unstable because of the lack of supervision far from S , we set $F_G = F_O$. Similarly, we choose $\delta_2 = 0.03$ in the definition of R_3 .

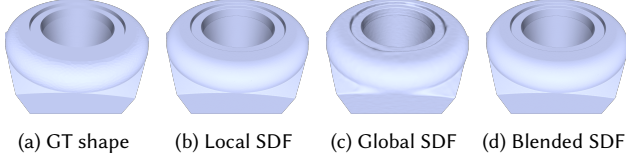


Fig. 13. A 3D local case that merges the local and global SDF fields to form a blended SDF. We visualize the zero-level sets of the local, global, and blended SDFs in (b), (c), and (d), respectively. The zero-level set of the blended SDF (d) is faithful to the GT shape (a).

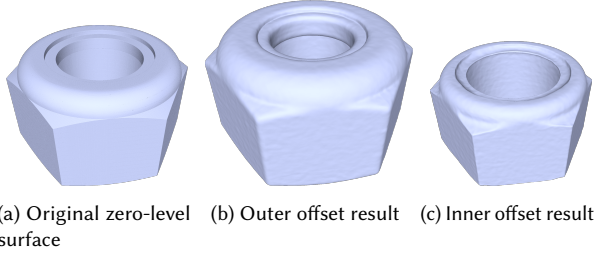


Fig. 14. Offset application (b and c) with the blended SDF whose zero-level set is shown in (a).

To make a smooth interpolation between F_L and F_O in R_2 , we first define the weight functions $w_0(s)$ and $w_1(s)$ so that

$$F_G(\mathbf{x}) = w_0 F_L(\mathbf{x}) + w_1 F_O(\mathbf{x}), \quad \mathbf{x} \in R_2. \quad (12)$$

Let us denote $d(\mathbf{x}) = |F_L(\mathbf{x})| \in [\delta_1, \delta_2]$, $\mathbf{x} \in R_2$ and $s(\mathbf{x}) = (d(\mathbf{x}) - \delta_1) / (\delta_2 - \delta_1)$ is a linear mapping maps $d(\mathbf{x})$ from $d(\mathbf{x}) \in [\delta_1, \delta_2]$ to $s(\mathbf{x}) \in [0, 1]$. We define the weight functions by

$$w_0(s) = (1 - h(s(x))), w_1(s) = h(s(x))$$

where $h(s) = 3s^2 - 2s^3$, for $s \in [0, 1]$; see Fig. 12.

Clearly, $h(0) = h'(0) = h'(1) = 0$ and $h(1) = 1$, from which one can verify that $F_G(\mathbf{x}) = F_L(\mathbf{x})$ and $\nabla F_G(\mathbf{x}) = \nabla F_L(\mathbf{x})$ along the inner boundaries of R_2 (i.e. where $|F_L(\mathbf{x})| = \delta_1$), and that $F_G(\mathbf{x}) = F_O(\mathbf{x})$ and $\nabla F_G(\mathbf{x}) = \nabla F_O(\mathbf{x})$ along the outer boundaries of R_2 (i.e. where $|F_L(\mathbf{x})| = \delta_2$). That is, F_G thus defined is an C^1 -continuous extension of F_L in $R_2 \cup R_3$. To summarize, the distance function $F_G(\mathbf{x})$ is a smooth blending of $F_L(\mathbf{x})$ and $F_O(\mathbf{x})$ and is globally defined on D . In particular, the zero-level set of F_G agrees with that of $F_L(\mathbf{x})$, so it preserves the sharp features of the original target surface.

Finally, we show a 3D result of our blending strategy in Fig. 13 and demonstrate an offset application of our global distance function F_G in Fig. 14.

5 EXPERIMENTAL RESULTS

5.1 Implementation details

Dataset and preprocessing. We test our method primarily on a data collection consisting of 100 CAD models sampled from the ABC dataset [Koch et al. 2019]. All the shapes are segmented in advance and normalized to $[-1, 1]^3$. For each segment of a given shape, we first construct a patch volume V_p . The resolution of the patch volume is determined by the average shape diameter [Shapira et al.

2008] of this segment computed with LIBIGL [Jacobson et al. 2018]. Specifically, we stipulate that the size of the patch grid allocated to each patch should not exceed 2.5 times the average shape diameter of the patch. We observe that the resolution of a patch feature volume ranges from 2^3 to 2^6 depending on the local feature size. We construct the merge grid \mathcal{G} as described in Sec. 3 and derive the merge constraints from the merge grid cells accordingly. We empirically set the maximal depth of the merge grid octree to 7.

Pretraining for shape update. In practice, it is often necessary to edit a 3D shape and update its corresponding implicit representation as well. Typically, the editing involves only a few patches. Therefore, to reuse the previously learned feature volumes while updating only the changed ones, we adopt the test-time optimization scheme, similar to [Park et al. 2019], to only update the patch feature volumes of the edited patches with the pretrained decoder fixed. We also allow using the fixed pretrained decoder to fit a completely new shape, which is denoted as *Patch-Grid-PT*. In this case, feature volumes of all patches are learnable.

Training details. We set the balance weights for the training loss terms as follows: $\lambda_{\text{surface}} = 150$, $\lambda_{\text{normal}} = 50$, $\lambda_{\text{SDF}} = 50$, $\lambda_{\text{gradient}} = 12$, $\lambda_{\text{off}} = 9$, $\lambda_{\text{eikonal}} = 12$, $\lambda_{\text{code}} = 1$, $\lambda_{\text{merge}} = 8$. We implemented the proposed method with PyTorch. ADAM [Kingma and Ba 2015] with default hyperparameters is used as the optimizer for both pretraining and the fitting stages. Our fitting results were trained using 300 iterations. With an initial learning rate of 0.001, the learning rate is decayed by a factor of 0.3 at the 270th and 285th iterations. This training process takes about 8 seconds to fit a shape from scratch. For shape updating, our results were trained using 80 iterations with the same learning rate decay scheme at the 65-th and 72-th iterations. In each iteration, we globally sample 10,000 surface points and 10,000 spatial points off the surface and assign the sampled points to their corresponding cells. All results produced by our *Patch-Grid* and by the comparing methods were obtained on a desktop with a GPU card of NVIDIA RTX4090 and Intel i9 13900kf CPU. More implementation details can be found in our codes.

5.2 Evaluation metrics

To evaluate fitting accuracy, we use the following metrics: 1) the symmetric Chamfer distance (CD); 2) the F-score based on CD; 3) the Hausdorff distance (HD); and 4) the normal consistency (NC). The symmetric Chamfer distance measures the averaged reconstruction quality of a given shape. The Hausdorff distance is the maximum reconstruction error either from the reconstruction to the ground-truth (GT) mesh or from the GT mesh to the reconstruction. The normal consistency measures how similar the normal vectors at the reconstructed surface are to those at the GT mesh surface. We also report F-score, a statistical measure, to show the overall quality of the reconstruction quality. Specifically, the F-score is computed as the percentage of points with a reconstruction error smaller than 0.001 throughout the paper. In all experiments, we sample 300k points from the extracted surface and another 300k from the ground-truth mesh. Then we compute the two-sided closest point-to-surface distances to evaluate all metrics.

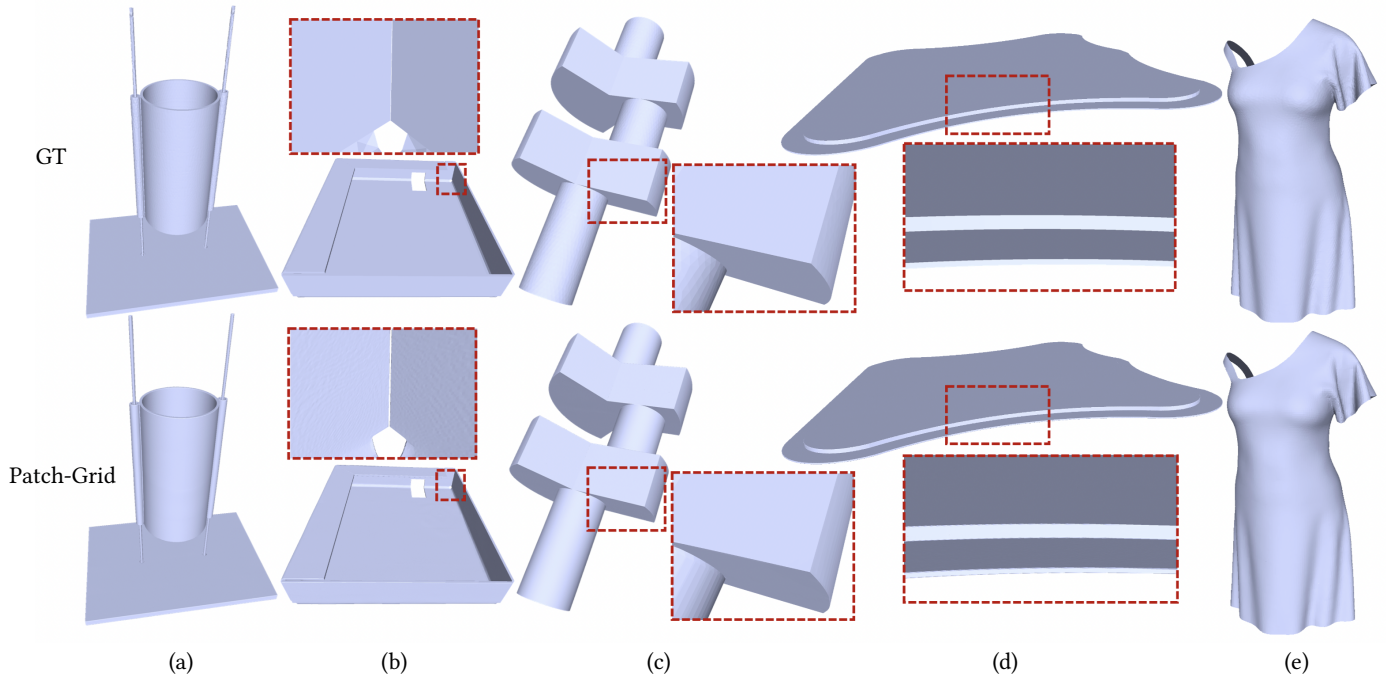


Fig. 15. Our proposed approach, *Patch-Grid*, is capable of representing shapes that possess various types of features and demonstrates exceptional accuracy and robustness. (a, b): thin structures; (c, d): sharp boundary edges and corners; (e): clean boundary curves in the open surfaces.

5.3 Results and discussions

Shape fitting. Our method can model 3D surface shapes with various geometry features, e.g., narrow gaps, sharp features, or open boundaries, at high fidelity as is shown in Fig 1(a) and Fig. 15.

We report the quantitative results in Tab. 1 produced by two variants of our approach (*Patch-Grid* and *Patch-Grid-PT*) and the state-of-the-art (SOTA) methods and compare them to the results produced by *NH-Rep* [Guo et al. 2022] and *NGLOD* [Takikawa et al. 2021] on two subsets of shapes randomly drawn from the ABC dataset, respectively. A subset of 100 shapes is used in the comparison with *NH-Rep*, whereas 10 shapes are randomly sampled for the comparison with *NGLOD* due to its prolonged training time. *Patch-Grid* denotes training our approach trained from scratch, while *Patch-Grid-PT* denotes training our approach with a fixed, pretrained decoder as described in the previous subsection. For the methods tested on the pool of 10 shapes, we added a suffix of * to denote them as *NGLOD**, *Patch-Grid**, and *Patch-Grid-PT**.

Our approach, in both its variants (*Patch-Grid* and *Patch-Grid-PT*), can achieve significantly better reconstruction performance than *NH-Rep* and *NGLOD* as indicated by the metrics. As we noted that there are some severe failure cases in *NH-Rep* due to its robustness issue as discussed earlier, we do not include these shapes in the quantitative comparison, and our approach still performs favorably as compared to *NH-Rep*. We attribute this performance gain to the use of the adaptive merge grid, which circumvents the difficulty in managing the extended zero-level sets of the learned patches to satisfy the global CSG constraints.

The training time for an object is typically around 8 seconds, taking 300 iterations, which is 23 \times and 287 \times speed-up as compared with *NH-Rep* (3 minutes) and *NGLOD* (38 minutes), respectively. Hence, our method brings about a significant improvement over the other comparing methods in both computational efficiency and fitting accuracy.

Table 1. Quantitative evaluation of different neural implicit representations in terms of the symmetric Chamfer distance (CD), F-score (CD < 0.001), Hausdorff distance (HD), and normal consistency (NC). \uparrow indicates the higher the better, while \downarrow indicates the lower the better. CD, HD and NC are presented in units of $\times 10^{-4}$, $\times 10^{-3}$ and $\times 10^{-2}$, respectively. We also report the training time in the unit of seconds.

Metrics	CD \downarrow	F-score \uparrow	HD \downarrow	NC \downarrow	Time \downarrow
NH-Rep	6.7	92.44	6.9	6.791	185
Patch-Grid	1.0	99.19	3.0	6.464	8
Patch-Grid-PT	1.5	99.39	2.7	6.430	8
NGLOD*	2.7	97.99	3.8	10.15	2296
Patch-Grid*	0.7	99.75	1.4	4.841	8
Patch-Grid-PT*	1.6	99.85	1.5	5.412	8

For qualitative comparison, we show several results produced by *Patch-Grid* and the other methods in Fig. 16. Compared with *NH-Rep* which also uses a patch-wise representation, *Patch-Grid* can robustly model geometric features presented in shapes as shown in the bottom two rows of Fig. 16. *NH-Rep* adopts a global approach

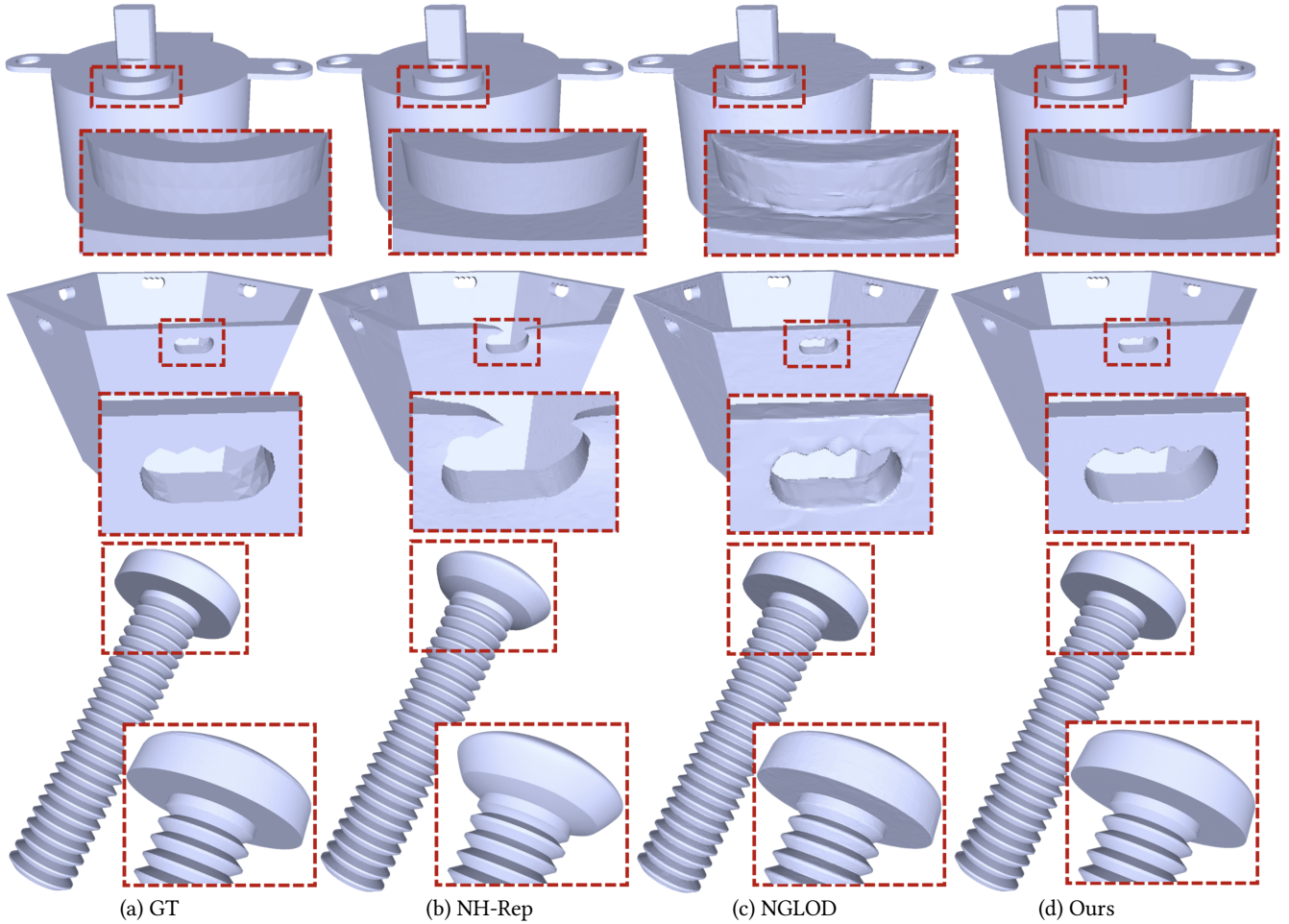


Fig. 16. Comparison with *NH-Rep* [Guo et al. 2022] and *NGLOD* [Takikawa et al. 2021]. *Patch-Grid* and *NH-Rep*, which adopt a patch-based representation, can faithfully capture sharp geometric features presented in the shapes, while *NGLOD* fails to do so, as shown in all the zoom-in views. Compared with *NH-Rep*, our local approach ensures robust performance in the presence of thin geometric features (in rows 2 and 3) that *NH-Rep* fails due to its global approach. The results produced by our method were obtained through an 8-second training phase, which demonstrates the efficiency of our method.

to assembling the learned implicit functions into the target shape, which is prone to fail due to the undesirable interference between the extraneous zero-level sets of the individual learned implicit patches. In contrast, *Patch-Grid* consistently produces robust, high-quality results even in these challenging cases, validating the superiority of the proposed local approach.

We also compare *Patch-Grid* to *NGLOD*, which models the entire shape without decomposition. Different from *NGLOD*, both *NH-Rep* and *Patch-Grid* are based on patch decomposition and therefore can faithfully model the sharp features presented in the 3D shapes as shown in the zoom-in views in Fig. 17. Here, we visualize the reconstruction error maps of our results and those of *NGLOD* regarding five additional shapes, which show that *Patch-Grid* consistently obtains smaller fitting errors for the five shapes than *NGLOD*. This superior accuracy is attributed to the use of patch-based representation, partly because it reduces our learning task to fit a small number

of patches in each merge grid cell locally instead of modeling a complex shape as is done for *NGLOD* and partly because *Patch-Grid* is capable of sharp features by composing several learned patches.

In addition to the CAD models and those models with thin geometric features in Figs. 7, we also show in Fig. 18 the reconstruction results of three garment models (i.e., a dress from VTO [Santesteban et al. 2019] and a shirt and a pair of pants from MGN [Bhatnagar et al. 2019]) with open surface boundaries to demonstrate the representational capability of the proposed method for modeling open surface boundaries. As shown, *Patch-Grid* produces accurately reproduces the open surface boundaries.

Shape editing. We have demonstrated a few updated shapes in Fig. 1(b) earlier. Now we show more shape updating results in Fig. 19. All the results are shown in Fig. 1(b) and Fig. 19 take only 1 second of training to complete with the *Patch-Grid-PT* setting where only the feature volumes of the edited patches were updated.

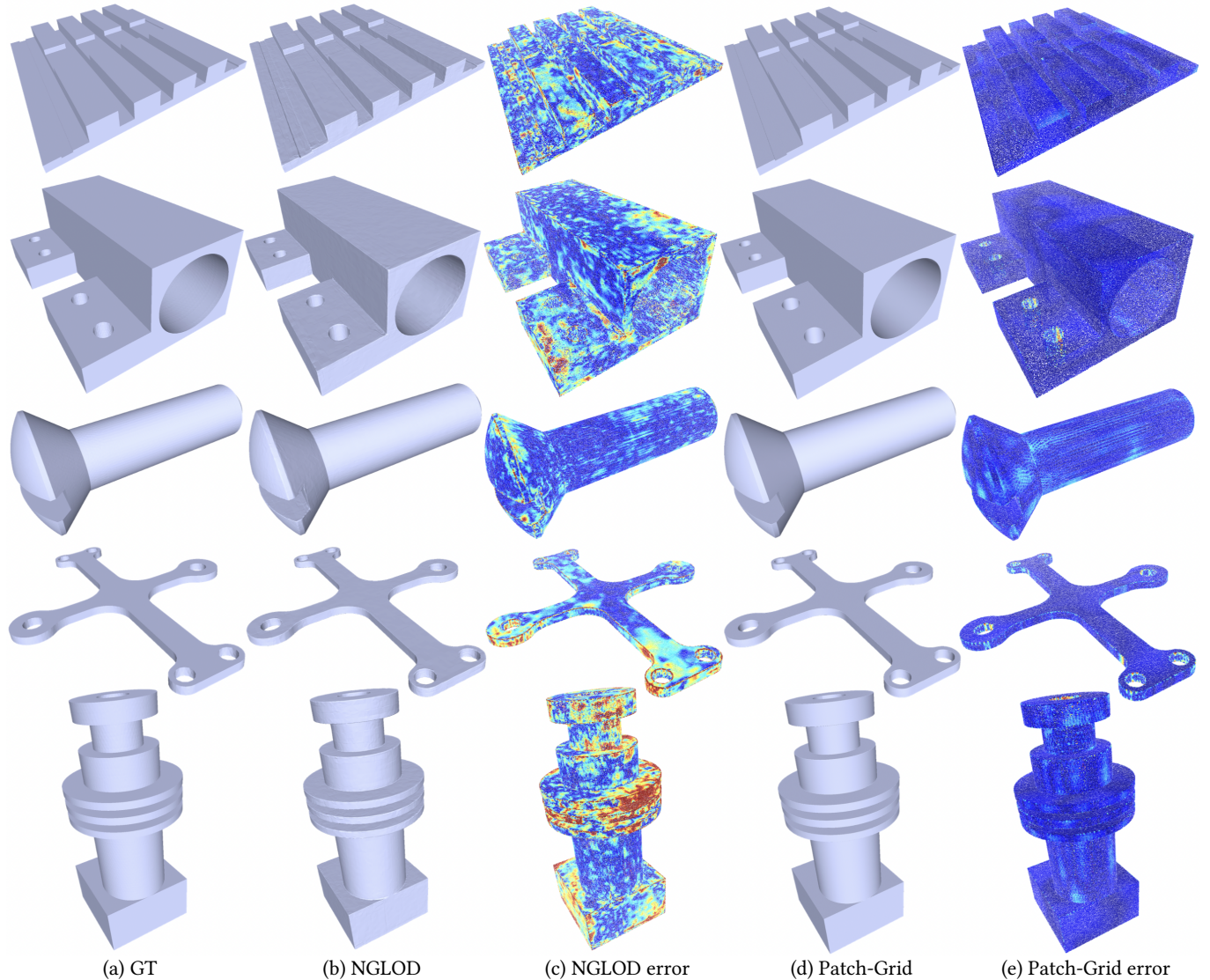


Fig. 17. Detailed comparison with *NGLOD* [Takikawa et al. 2021]. Columns (c) and (e) show the error distributions in terms of the Chamfer Distance between the reconstructed and GT meshes by *NGLOD* and *Patch-Grid*, respectively. The warmer color indicates a higher error, with the error being clipped by 0.001. *Patch-Grid* outperforms *NGLOD* significantly in terms of fitting accuracy, especially around the sharp features of the presented shapes.

We applied a variety of editing operations to the shape shown in Fig. 19, such as adding a trimming surface to form a chamfer to the central hole as in Fig. 19(e). In each edited shape, we highlight the modified patches in orange. Additionally, the connected patches that are not directly edited but are affected by the update of the merge constraints are highlighted in green. Both the edited and involved patches are updated while the rest of the patches are kept fixed.

The fitting accuracy regarding these edited shapes is reported in Tab. 2, which is similar to the performance obtained in the shape fitting task, demonstrating the consistently superior performance of our method in both shape fitting and updating tasks.

Table 2. Quantitative evaluation of the edited shapes. The accuracy of the edited shape is consistent with the accuracy of shape fitting. CD, HD and NC are presented in units of $\times 10^{-4}$, $\times 10^{-3}$ and $\times 10^{-2}$, respectively. The training time is in the unit of seconds.

CD ↓	F-score ↑	HD ↓	NC ↓	Time ↓
1.8	98.84	3.1	3.504	1

5.4 Ablation study

We conducted ablation studies to validate the use of the adaptive patch volumes by ablating this design choice, denoted *w/o Ada-PV*.

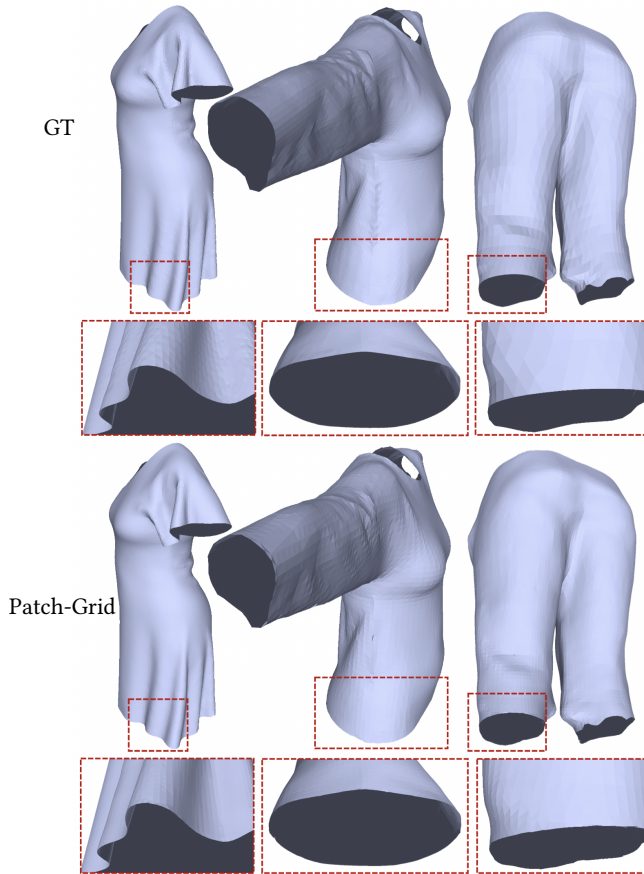


Fig. 18. Examples of open surfaces with the zoom-in views at the open surface boundaries. *Patch-Grid*, modeling the open surface boundaries via a trimming process, cuts the boundaries in a precise and clean manner.

Tab. 3 shows that *w/o Ada-PV* yields less satisfactory results. A qualitative example is provided in Fig. 21 to show the necessity of adaptive patch volumes for modeling slender geometry; otherwise, using patch volumes of uniform size fails to accurately fit thin tubes.

Regarding the two previously introduced training schemes: 1) with a trainable decoder from scratch; and 2) with a fixed pretrained decoder, we conducted an experiment to show their respective advantages. Both schemes were used to fit the data collection of 100 shapes and the results are reported Tab. 3. We see that training the decoder from scratch (i.e., scheme 1) can achieve slightly favorable results in terms of the Chamfer distance and F-score. Yet, Scheme 1 (*Train from Scratch*) converges slower (around 300 iterations, or 8 seconds) than Scheme 2 (*Fixed decoder*) which requires around 100 iterations, or 3 seconds as shown in Fig. 20.

6 CONCLUSION

We have presented a novel implicit neural surface using a patch-based representation with a grid-based local training and merging strategy. *Patch-Grid* performs CSG operations locally in grid-based cells to significantly improve the robustness of the patch-based

Table 3. Quantitative results of the ablation. It shows using adaptive resolutions for different patch volumes leads to better performance. Similar performance gain can be achieved by the two variants of our method. CD, HD and NC are presented in units of $\times 10^{-4}$, $\times 10^{-3}$ and $\times 10^{-2}$, respectively.

	CD ↓	F-score ↑	HD ↓	NC ↓
Train from Scratch	1.0	99.19	3.0	6.464
Fixed decoder	1.5	99.39	2.7	6.430
w/o Ada-PV	7.7	98.56	12	6.608

representation, compared with the prior work [Guo et al. 2022] using a global approach. Moreover, *Patch-Grid* is capable of dealing with a wide variety of shapes including thin geometries, open surfaces. We evaluate *Patch-Grid* on various 3D shapes to validate its superiority to existing works in terms of robustness, efficiency, accuracy, and versatility.

There are several limitations to our method. (1) *Patch-Grid* assumes a preprocessing stage that provides us with meaningful segmentation for models. A shape segmentation procedure is needed as a preprocessing step for our method. (2) Currently, *Patch-Grid* cannot represent non-manifold surfaces, which is a task that would need further research. Furthermore, it is an interesting topic for future research to explore the potential of *Patch-Grid* to support structure-level or semantic-level shape editing and shape manipulation due to its flexible representation with patch-wise latent spaces.

REFERENCES

- George Allen. 2021. nTopology’s Implicit Modeling Technology. <https://ntopology.com/resources/whitepaper-implicit-modeling-technology/>. Last accessed 2021-12-1.
- Nina Amenta and Marshall Bern. 1998. Surface reconstruction by Voronoi filtering. In *Proceedings of the fourteenth annual symposium on Computational geometry*. 39–48.
- Bharat Lal Bhatnagar, Garvita Tiwari, Christian Theobalt, and Gerard Pons-Moll. 2019. Multi-Garment Net: Learning to Dress 3D People from Images. In *IEEE International Conference on Computer Vision (ICCV)*. IEEE.
- Weikai Chen, Cheng Lin, Weiyang Li, and Bo Yang. 2022. 3PSDF: Three-Pole Signed Distance Function for Learning Surfaces With Arbitrary Topologies. In *Proceedings of the IEEE/CVF Conference on Computer Vision and Pattern Recognition (CVPR)*. 18522–18531.
- Zhiqin Chen and Hao Zhang. 2019. Learning Implicit Fields for Generative Shape Modeling. In *Proceedings of the IEEE/CVF Conference on Computer Vision and Pattern Recognition (CVPR)*.
- Julian Chibane, Mohamad Aymen mir, and Gerard Pons-Moll. 2020. Neural Unsigned Distance Fields for Implicit Function Learning. In *Advances in Neural Information Processing Systems*, H. Larochelle, M. Ranzato, R. Hadsell, M.F. Balcan, and H. Lin (Eds.), Vol. 33. Curran Associates, Inc., 21638–21652. <https://proceedings.neurips.cc/paper/2020/file/f69e505b08403ad2298b9f262659929a-Paper.pdf>
- Thomas Davies, Derek Nowrouzezahrai, and Alec Jacobson. 2020. On the Effectiveness of Weight-Encoded Neural Implicit 3D Shapes. <https://doi.org/10.48550/ARXIV.2009.09808>
- Yueqi Duan, Haidong Zhu, He Wang, Li Yi, Ram Nevatia, and Leonidas J. Guibas. 2020. Curriculum DeepSDF. In *Computer Vision – ECCV 2020*, Andrea Vedaldi, Horst Bischof, Thomas Brox, and Jan-Michael Frahm (Eds.). Springer International Publishing, Cham, 51–67.
- Kyle Genova, Forrester Cole, Avneesh Sud, Aaron Sarna, and Thomas Funkhouser. 2020. Local Deep Implicit Functions for 3D Shape. In *Proceedings of the IEEE/CVF Conference on Computer Vision and Pattern Recognition (CVPR)*.
- Amos Gropp, Lior Yariv, Niv Haim, Matan Atzmon, and Yaron Lipman. 2020. Implicit Geometric Regularization for Learning Shapes. In *Proceedings of the 37th International Conference on Machine Learning (Proceedings of Machine Learning Research, Vol. 119)*, Hal Daumé III and Aarti Singh (Eds.). PMLR, 3789–3799. <https://proceedings.mlr.press/v119/gropp20a.html>
- Hao-Xiang Guo, Yang Liu, Hao Pan, and Baining Guo. 2022. Implicit Conversion of Manifold B-Rep Solids by Neural Halfspace Representation. *ACM Trans. Graph.* 41,

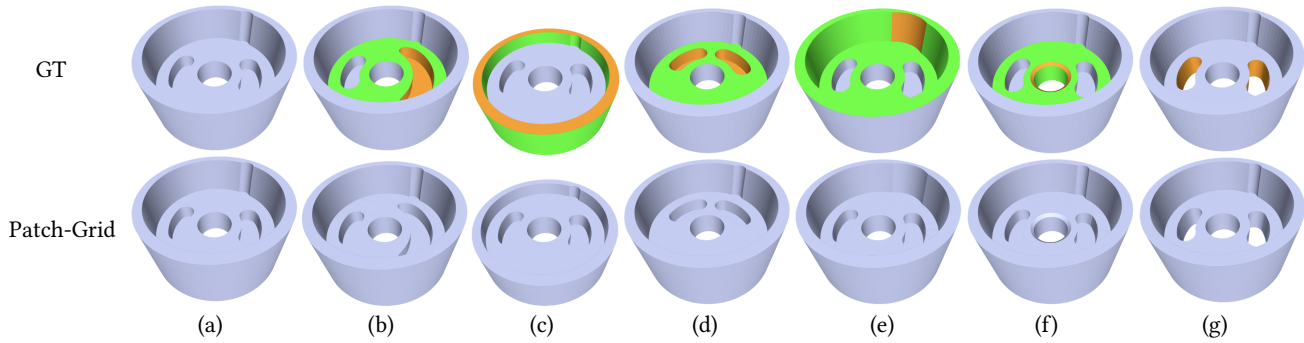


Fig. 19. A collection of edited shapes (top) and the results (bottom) fitted by our shape updating strategy is presented. A variety of editing operations are applied to the original shape in (a). (b): free-form deformation of the circular slot; (c): parametric editing of the height of the top; (d) rigid transformation of the pair of circular slots; (e): parametric editing of the radius of the cylindrical patch; (f): adding a new patch to create a chamfer to the central through-hole; (g): Extending several patches and removing two patches to obtain a pair of penetrated slots. In each edited shape, the modified patches are highlighted in orange. Additionally, the connected patches that are not directly edited but are affected by the changes due to merge constraints are also highlighted in green. Patch feature volumes of both the directly edited and affected patches are updated while the rest of the patch feature volumes remain fixed.

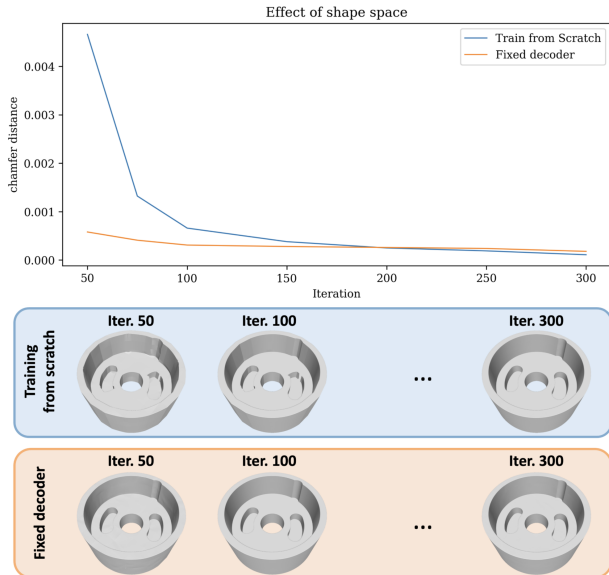


Fig. 20. Pretrained fixed shape space matters. The ablation reveals that the use of a fixed, pretrained decoder significantly accelerates training as shown by the curves of CD value against the number of iterations (around 100 iterations). In contrast, without pretraining, our method takes 200 iterations to converge. The impact of the pretrained shape space is also evident in the visualization of the shapes, as demonstrated in the following figures.

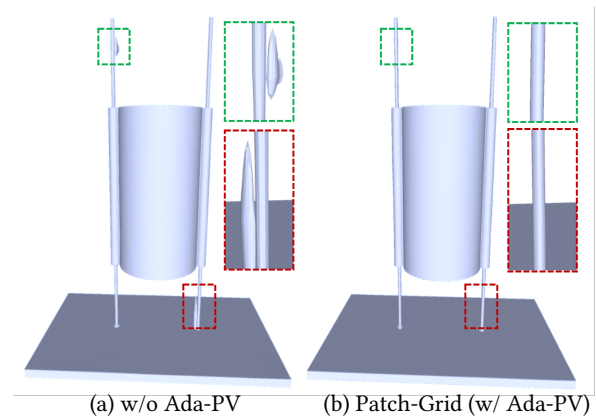


Fig. 21. Adaptive patch volumes matter. (a) Without the use of adaptive patch volumes, the resulting shape extracted from the compositional neural signed distance field may have artifacts observed around the thin components due to the uniform resolution used across different patches; (b) Using adaptive patch volumes can effectively resolve the issue, showing the necessity for the proposed method.

6, Article 276 (nov 2022), 15 pages. <https://doi.org/10.1145/3550454.3555502>
 Alec Jacobson, Daniele Panozzo, et al. 2018. libigl: A simple C++ geometry processing library. <https://libigl.github.io/>.
 Chiyu "Max" Jiang, Ameesh Sud, Ameesh Makadia, Jingwei Huang, Matthias Niessner, and Thomas Funkhouser. 2020. Local Implicit Grid Representations for 3D Scenes. In *Proceedings of the IEEE/CVF Conference on Computer Vision and Pattern Recognition (CVPR)*.
 Diederik P. Kingma and Jimmy Ba. 2015. Adam: A Method for Stochastic Optimization. In *3rd International Conference on Learning Representations, ICLR 2015, San Diego, CA, USA, May 7-9, 2015, Conference Track Proceedings*, Yoshua Bengio and Yann

LeCun (Eds.). <http://arxiv.org/abs/1412.6980>
 Sebastian Koch, Albert Matveev, Zhongshi Jiang, Francis Williams, Alexey Artemov, Evgeny Burnaev, Marc Alexa, Denis Zorin, and Daniele Panozzo. 2019. ABC: A Big CAD Model Dataset for Geometric Deep Learning. In *Proceedings of the IEEE/CVF Conference on Computer Vision and Pattern Recognition (CVPR)*.
 Yangyan Li, Xiaoqun Wu, Yiorgos Chrysathou, Andrei Sharf, Daniel Cohen-Or, and Niloy J. Mitra. 2011. GlobFit: Consistently Fitting Primitives by Discovering Global Relations. In *ACM SIGGRAPH 2011 Papers* (Vancouver, British Columbia, Canada) (SIGGRAPH '11). Association for Computing Machinery, New York, NY, USA, Article 52, 12 pages. <https://doi.org/10.1145/1964921.1964947>
 Julien NP Martel, David B Lindell, Connor Z Lin, Eric R Chan, Marco Monteiro, and Gordon Wetzstein. 2021. ACORN: Adaptive Coordinate Networks for Neural Scene Representation. *arXiv preprint arXiv:2105.02788* (2021).
 Lars Mescheder, Michael Oechsle, Michael Niemeyer, Sebastian Nowozin, and Andreas Geiger. 2019. Occupancy Networks: Learning 3D Reconstruction in Function Space. In *Proceedings of the IEEE/CVF Conference on Computer Vision and Pattern Recognition (CVPR)*.
 Nathan Mitchell, Mridul Aanjaneya, Rajsekhar Setaluri, and Eftychios Sifakis. 2015. Non-manifold level sets: A multivalued implicit surface representation with applications

- to self-collision processing. *ACM Transactions on Graphics (TOG)* 34, 6 (2015), 1–9.
- Thomas Müller, Alex Evans, Christoph Schied, and Alexander Keller. 2022. Instant neural graphics primitives with a multiresolution hash encoding. *ACM Transactions on Graphics (ToG)* 41, 4 (2022), 1–15.
- Liangliang Nan and Peter Wonka. 2017. PolyFit: Polygonal Surface Reconstruction From Point Clouds. In *Proceedings of the IEEE International Conference on Computer Vision (ICCV)*.
- Yutaka Ohtake, Alexander Belyaev, Marc Alexa, Greg Turk, and Hans-Peter Seidel. 2005. Multi-level partition of unity implicits. In *Acm Siggraph 2005 Courses*. 173–es.
- Jeong Joon Park, Peter Florence, Julian Straub, Richard Newcombe, and Steven Lovegrove. 2019. DeepSDF: Learning Continuous Signed Distance Functions for Shape Representation. In *Proceedings of the IEEE/CVF Conference on Computer Vision and Pattern Recognition (CVPR)*.
- Igor Santesteban, Miguel A. Otaduy, and Dan Casas. 2019. Learning-Based Animation of Clothing for Virtual Try-On. *Computer Graphics Forum (Proc. Eurographics)* (2019). <https://doi.org/10.1111/cgf.13643>
- R. Schnabel, R. Wahl, and R. Klein. 2007. Efficient RANSAC for Point-Cloud Shape Detection. *Computer Graphics Forum* 26, 2 (2007), 214–226. <https://doi.org/10.1111/j.1467-8659.2007.01016.x> arXiv:<https://onlinelibrary.wiley.com/doi/pdf/10.1111/j.1467-8659.2007.01016.x>
- Lior Shapira, Ariel Shamir, and Daniel Cohen-Or. 2008. Consistent mesh partitioning and skeletonisation using the shape diameter function. *The Visual Computer* 24 (2008), 249–259.
- Vincent Sitzmann, Eric R Chan, Richard Tucker, Noah Snavely, and Gordon Wetzstein. 2020a. Metasdf: Meta-learning signed distance functions. *arXiv preprint arXiv:2006.09662* (2020).
- Vincent Sitzmann, Julien Martel, Alexander Bergman, David Lindell, and Gordon Wetzstein. 2020b. Implicit Neural Representations with Periodic Activation Functions. In *Advances in Neural Information Processing Systems*, H. Larochelle, M. Ranzato, R. Hadsell, M.F. Balcan, and H. Lin (Eds.), Vol. 33. Curran Associates, Inc., 7462–7473. <https://proceedings.neurips.cc/paper/2020/file/53c04118df112c13a8c34b38343b9c10-Paper.pdf>
- Towaki Takikawa, Joey Litalien, Kangxue Yin, Karsten Kreis, Charles Loop, Derek Nowrouzezahrai, Alec Jacobson, Morgan McGuire, and Sanja Fidler. 2021. Neural Geometric Level of Detail: Real-Time Rendering With Implicit 3D Shapes. In *Proceedings of the IEEE/CVF Conference on Computer Vision and Pattern Recognition (CVPR)*. 11358–11367.
- Matthew Tancik, Pratul Srinivasan, Ben Mildenhall, Sara Fridovich-Keil, Nithin Raghavan, Utkarsh Singhal, Ravi Ramamoorthi, Jonathan Barron, and Ren Ng. 2020a. Fourier Features Let Networks Learn High Frequency Functions in Low Dimensional Domains. In *Advances in Neural Information Processing Systems*, H. Larochelle, M. Ranzato, R. Hadsell, M.F. Balcan, and H. Lin (Eds.), Vol. 33. Curran Associates, Inc., 7537–7547. <https://proceedings.neurips.cc/paper/2020/file/55053683268957697aa39fba6f231c68-Paper.pdf>
- Matthew Tancik, Pratul P Srinivasan, Ben Mildenhall, Sara Fridovich-Keil, Nithin Raghavan, Utkarsh Singhal, Ravi Ramamoorthi, Jonathan T Barron, and Ren Ng. 2020b. Fourier features let networks learn high frequency functions in low dimensional domains. *arXiv preprint arXiv:2006.10739* (2020).
- Edgar Tretschk, Ayush Tewari, Vladislav Golyanik, Michael Zollhöfer, Carsten Stoll, and Christian Theobalt. 2020. PatchNets: Patch-Based Generalizable Deep Implicit 3D Shape Representations. In *Computer Vision – ECCV 2020*, Andrea Vedaldi, Horst Bischof, Thomas Brox, and Jan-Michael Frahm (Eds.). Springer International Publishing, Cham, 293–309.
- Greg Turk and James F O'brien. 2002. Modelling with implicit surfaces that interpolate. *ACM Transactions on Graphics (TOG)* 21, 4 (2002), 855–873.
- Congyi Zhang, Mohamed Elgharib, Gereon Fox, Min Gu, Christian Theobalt, and Wenping Wang. 2022. An Implicit Parametric Morphable Dental Model. *ACM Trans. Graph.* 41, 6, Article 217 (nov 2022), 13 pages. <https://doi.org/10.1145/3550454.3555469>